Industrial Health 2018, **56**, 475–484

Original Article

Unstable behavior of segmental ring under various pressures and its discrete element simulation

Naotaka KIKKAWA[1]*, Nobutaka HIRAOKA[1], Kazuya ITOH[2] and Rolando P. ORENSE[3]

[1]Construction Safety Research Group, National Institute of Occupational Safety and Health, Japan
[2]Department of Urban and Civil Engineering, Tokyo City University, Japan
[3]Department of Civil and Environmental Engineering, University of Auckland, New Zealand

Received February 27, 2018 and accepted June 13, 2018
Published online in J-STAGE June 23, 2018

Abstract: In February 2012, a serious accident which resulted in five fatalities happened during a TBM-tunnel construction under the seabed in Japan. The cause of the accident appeared to be due to the Key-segment slipping out of the segment ring by the thrusting tailskin (wire brushes) of the TBM into the segment ring. This resulted in the collapse of the rings, causing the seabed ground and seawater to flow into the tunnel. We investigated how thin and thick segments without any circumferential joints behave under isotropic and anisotropic pressures using small-scale physical model. In the model tests, pressures were applied to the surroundings of the segment rings and the strains at each segment were measured in order to evaluate the damage. In addition, cases where lubrication on the contact area between the K- and B-segments was present or not were investigated and their discrete element simulations were also conducted.

Key words: TBM tunnel construction, Segmental ring, Anisotropic pressure, Discrete Element Simulation, Stress-strain relationship

Introduction

TBM-tunnels are generally designed considering both earth and water pressures acting on the condition that the segmental rings are completely formed. Thus, it is rare to observe some deformation/damage suffered mainly due to the lack of structural strength of the segment rings against earth and water pressures after a TBM tunnel has been completed. During construction works, however, segments may suffer additional pressure, say from the thrusting tail-skin (wire brushes) of the TBM[1)] and from the thrust cylinder itself of the TBM[2)] to name a few.

In February 2012, a serious accident which resulted in five fatalities happened during a TBM-tunnel construction under the seabed in Japan[3)]. When the 112th segmental ring was formed inside the TBM where the tail-skin was shorter at that site, half of the 111th segment ring which was previously installed would be outside the TBM, so that the stability of the 111th segment ring was very significant with around half of the segment which was 1,400 mm wide was subjected to earth/water pressure. At that time, the thrust cylinders were pulling back from the 111th segment as the 112th segmental ring was being installed. At this moment, portions of the 111th segment were not adequately supported along the direction of the tunnel progress. Then, since the circumferential joints between K- and B-segments had bolt-less joints and the contact areas between them were lubricated, the K-segment slipped out of the 111th segment ring. As a result, the 111th and 110th segment rings collapsed and then the seabed ground and seawater flowed into the tunnel.

*To whom correspondence should be addressed.
E-mail: kikkawa@s.jniosh.go.jp

In terms of dimensions, the outer diameter, inner diameter, width and thickness of one segmental ring were 4,820 mm, 4,500 mm, 1,400 mm and 160 mm, respectively. The segmental ring consisted of 5 segments, A1-, A2-, B1-, B2- and K-segments. The A- and B-segments had also boltless joints and the K-segment was inserted into the B-segments at an angle of 9.7 degrees.

Moreover, as another example, after the tunnel construction is completed and while the tunnel is being used for quite some time, the environment surrounding the tunnel could change. This could be due to the change in water level and this could cause segmental ring deformations/damages due to the differential pressure caused by changes in the surroundings of the tunnel.

In order to confirm if segments satisfy their required performance, simple bending test is generally carried out before the segment is installed into a TBM-tunnel construction site. The bending test is conducted by loading the central line of the outer diameter of the segment as an arch beam using movable bearings at both sides of the reinforced concrete segment[4]. The bending tests are separated into two types: one method involves loading horizontally and the other method is loading vertically. The former includes the effect of friction between the segment and the ground where the segment is placed, while the latter includes the effect of the self-weight of the segment due to gravity.

Various parameters, such as the maximum load, the load when the cracks are generated, the strain and the width of the cracks, are generally measured during the simple bending tests. Yuasa *et al.*[5] performed simple bending tests using reinforced concrete segments where they measured the width of the cracks during the tests and evaluated the waterproofness of the segments.

In this paper, in order to investigate the deformation behavior of segments under various pressures, we made a miniature physical model of the segment and a loading/unloading apparatus for the segmental ring after which we tried to measure the stress-strain behavior of each segment in a segmental ring. In addition, in order to evaluate the damage in a segment through its strain level, we applied the simple bending test on an intact segment and measured the load and strain on the segment. The strain level at failure in the simple bending test was compared to the strain level of segmental ring caused by various pressures from the loading/unloading apparatus.

Moreover, some of the experimental tests were simulated by using Discrete Element Method (DEM). In both experimental tests and numerical analyses, we focused on the stability of a single segment ring. Generally, the three-dimensional stability should be evaluated involving the direction of the tunnel progress, as the next segment ring is being connected to the previous one by bolts. However, before the three-dimensional effects could be discussed, the stability of a single segment ring needs to be checked as it is affected by the roundness of the subsequent segment rings and also by the tunnel alignment in three dimensions. Thus, we believed that the stability of a single segment ring is very important.

Table 1. Dimensions of the miniature segments

	Thin segment	Thick segment
Outer diameter (mm)	150	150
Inner diameter (mm)	140	130
Thickness (mm)	5	10
Width (mm)	43.8	43.8
Number of segments comprising the ring	5	5

Experiment and Simulation

In this paper, we constructed a miniature physical model of the segments and applied various pressures to the segments using a simple loading/unloading apparatus. Then we investigated the behavior of the segment itself and the stress-strain behavior of the segments.

Preparation procedure for miniature physical model of segments

The miniature segment ring consisted of five segments; these are referred to as A1-, A2-, B1-, B2- and K-segment, respectively. The outer diameter and width of the segment ring were 150 mm and 44 mm, respectively. We prepared two types of segments with different thicknesses, i.e. 5 mm and 10 mm thick. The dimensions of the miniature segments are summarized in Table 1. From the table, the ratios of the segment thickness to the outer diameter were 3.33% for the thin segment and 6.66% for the thick segment. Note that the standard ratio suggested in Japan is 4.00%.

The segmental ring was made by pouring cement grout into a mold, which was made of silicone rubber at the side of the outer and inner diameters of the segment and of acryl in the other parts, as shown in Fig. 1. As a method of separating the ring into each segment (A1, A2, B1, B2 and K), we made a cut into the silicone rubber at both sides and then inserted very thin copper plates (thickness of 0.2 mm) into the cut. The copper plates, shown in Fig. 2, functioned as partitions between segments.

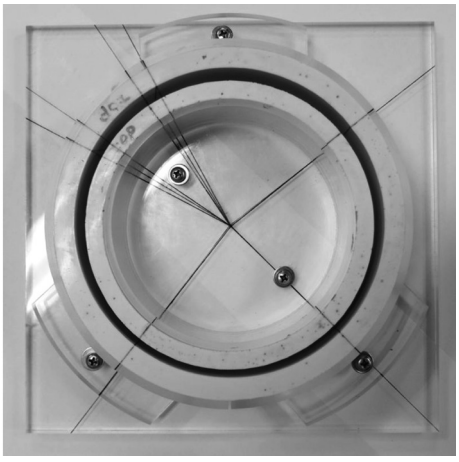

Fig. 1. Mold for making a small-scale physical model of segment (thickness of 5 mm).

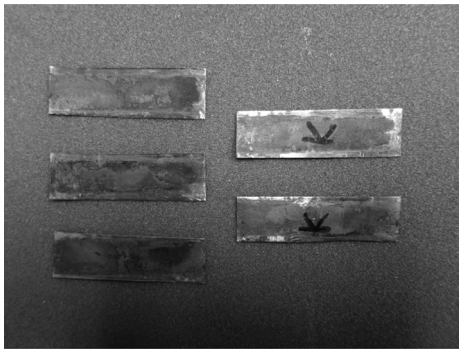

Fig. 2. Copper plates (0.2 mm thick) used as partitions between each segment.

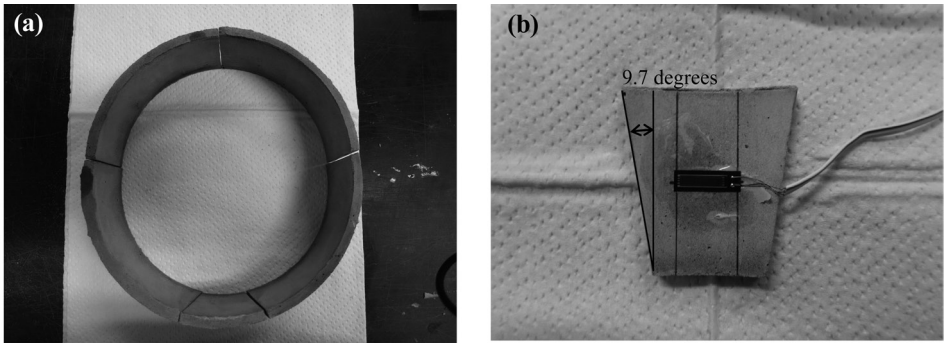

Fig. 3. Small-scale physical model of the segments (thickness of 5 mm). (a) Segmental ring, (b) K-segment (The angle of the sides of K-segment adjacent to the B-segments was 9.7 degrees).

As part of the preparation procedure, we poured the cement grout into the mold whose surface was coated with a mold-releasing agent. The cement grout consisted of high early-strength cement, Toyoura sand and water with a mass ratio of 1: 2: 0.65[6]. The mean unconfined compression strength of the specimen made with this composition was 46.2 N/mm^2, corresponding to the average of three specimens at a curing time of 28 days. In addition, we measured the ultrasonic wave propagation velocities, i.e. the P- and S-wave velocities of V_{p_bm}= 3,920 m/sec and V_{s_bm}= 2,340 m/sec, respectively. Next, the cement grout poured into the mold was densified while the air bubbles inside the cement grout were released as much as possible using a vibrator. After this, the mold was covered with a glass-plate into which the mold-releasing agent was applied and then some weights were mounted on the glass-plate. After a few days, we removed the segments from the mold and then we put the segments underwater. The total curing time was taken as 28 days after the cement grout was poured.

After curing, we pasted a strain gauge into the interior side of each segment for the purpose of measuring the strain at each segment under various pressures during testing. The images of the segments after curing are shown in Fig. 3.

Simple bending tests

In this study, an unconfined compression test apparatus[7] was used as the test apparatus for the simple bending test. The unconfined compression test apparatus is commonly used for concrete, soft-rock and clay. The function of the test apparatus is to load the test specimen by putting it on the bottom pedestal which is moving up toward the fixed top plate at a constant speed. The top plate has a spherical support that could reduce the concentration of loading to the specimen during the test. The simple bending test is usually carried out using two lines of loading; in this study, however, we applied only one line of loading using the top plate with the spherical support.

During the bending test, two teflon sheets were placed

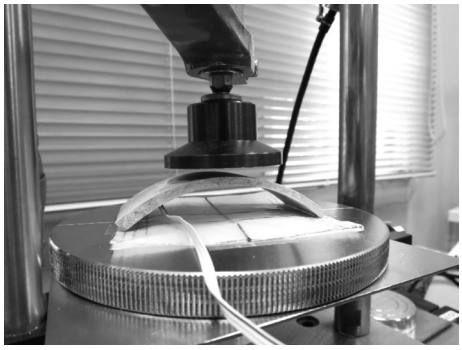

Fig. 4. Condition of A1-segment (thickness of segment: 5 mm) in simple bending test before loading.

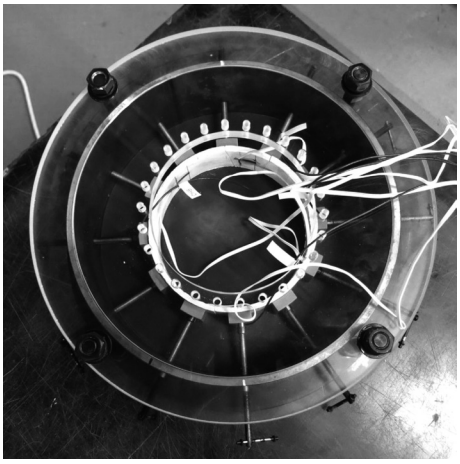

Fig. 5. Loading/unloading apparatus to test small-scale physical model of segments (thickness of 5 mm).

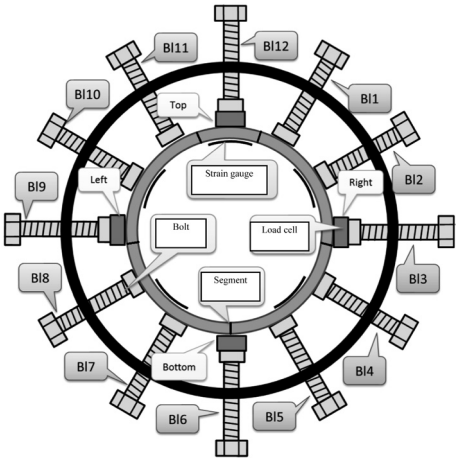

Fig. 6. Sketch of loading/unloading apparatus used to test small-scale physical model of segments.

at the bottom pedestal and then the miniature segment was mounted on the teflon sheets in order to reduce the friction between the segment and the pedestal. Next, the pedestal was moved up until the segment reached the top plate. After that, the pedestal was moved up at a constant speed of 1mm/min, and the segment was pressed to the top plate until the segment failed by bending. The load, displacement and strain were measured, respectively, by the load cell, external displacement transducer and strain gauge pasted on the inner diameter of the segment.

Figure 4 shows the condition of the simple bending test before loading.

Loading/unloading apparatus for segments

The loading/unloading apparatus was made of steel tube whose diameter was larger than that of the segmental ring. The circumference of the tube was drilled by a total of 12 bolts, wherein each bolt could be tightened/loosened to load/unload the segment ring. A photo and sketch of the apparatus are shown in Figs. 5 and 6, respectively.

Here, the arrangement of the bolts were made in the same way as that of the hours in a clock; the bolts were called Bl1, Bl2, Bl3, …, Bl12 in a clockwise manner, with Bl12 at the top. In addition, the end of some bolts was connected to a load cell, and the load cell and a steel arch plate (40 mm × 20 mm) were placed into the gap between the bolt and segment in order to prevent the concentration of loading and to monitor the pressure against the segments. The load cells were mounted on Bl3, Bl6, Bl9, Bl12 bolts.

Loading/unloading

We increased the pressure isotropically until 500 kN/m^2 and then decreased it also isotropically to 0 kN/m^2. Next, we increased the pressure isotropically again until 500 kN/m^2 and then only the bolts Bl8, Bl9, Bl10 were tightened further until a pressure of 700 kN/m^2 was reached. Thereafter, Bl8, Bl9, Bl10 were loosened until 500 kN/m^2 was achieved and then finally all the bolts were loosened isotropically until 0 kN/m^2.

With regards to the procedure of loading/unloading, when we tightened/loosened Bl6 and Bl12 initially, and then Bl3 and Bl9 by around 20 to 60 kN/m^2, the stresses in the load cells were monitored. After that, the number of revolutions of those bolts was recorded and the other bolts were also tightened using the same number of revolutions as the bolts Bl3, Bl6, Bl9 and Bl12 because the stresses in the other bolts were not monitored with load cells.

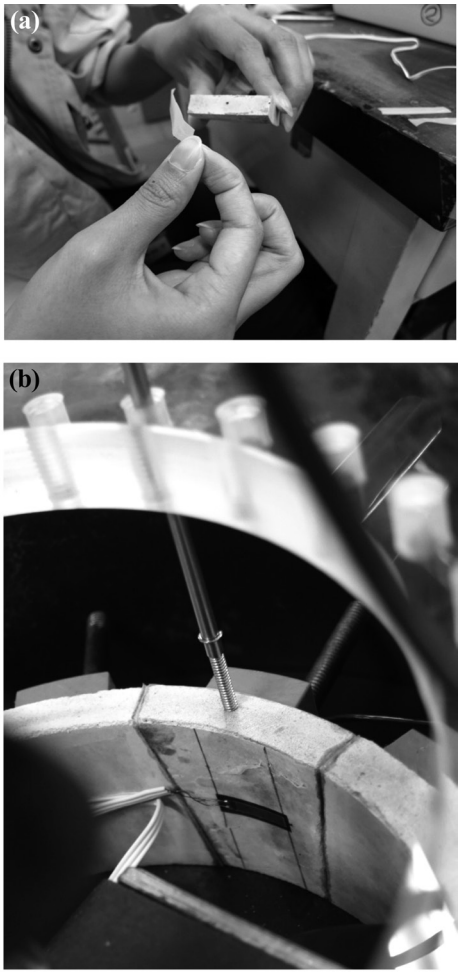

Fig. 7. Conditions of experimental tests on K-segment (Cases 3 and 4).
(a) Pasting of a teflon sheet and grease, (b) Mounting of displacement transducer on K-segment.

Regarding the TBM tunnel construction, the contact areas between K- and B-segments are typically lubricated in order to insert the K-segment easily into the partially assembled segmental ring and minimize the potential damage to the seal material pasted on the surface of the contact area between the segments. In this study, we also tested the case wherein K- and B-segments were lubricated. In the experimental tests, teflon sheets were pasted and lubricant was applied on both sides of the contact areas between K- and B-segments. During the tests, we also monitored the displacement of the K-segment while slipping out of the segment ring using a displacement transducer (Fig. 7).

The conditions of all experimental tests are summarized in Table 2.

Table 2. Conditions of the experimental tests

Case No.	Friction between segments	Thickness of segment
Case 1	Not lubricated	5 mm
Case 2	Not lubricated	10 mm
Case 3	Lubricated	5 mm
Case 4	Lubricated	10 mm

Numerical simulation

We simulated the experimental tests by using Discrete Element Method (DEM). In this paper, only the results for Case No. 3 in Table 2 are presented and the simulations of the other cases of experimental tests are still ongoing. In the simulation, the miniature segments were enlarged 32 times to represent full-scale segments with the following dimensions: 4,820 mm in outer diameter, 4,500 mm in inner diameter, 1,400 mm in width and 160 mm in thickness. The above dimensions satisfied the scaling law.

The preparation procedure of segments in the simulation was as follows:

(i) Set up the cylindrical wall elements with diameters that were similar to the outer and inner diameters of the segment ring.

(ii) Set-up the square wall elements that serve as the top and bottom plates of the segment ring in the direction of the segment width.

(iii) Generate sphere elements between the wall elements, with the following dimensions: 0.0272 mm minimum radius, 0.0544 mm maximum radius and 0.0408 mm mean radius.

(iv) Set-up the wall elements between the segments, as shown in Fig. 8 (a), with the wall elements positioned similar to those of the copper plates used in the experimental tests.

(v) Apply parallel-bonds between the sphere elements.

(vi) Remove the parallel-bonds only between the segments so that each segment was completely independent.

(vii) Remove the wall elements between the segments, the cylindrical wall elements and the square wall element acting as the top plate of the segment ring in the direction of the segment width.

(viii) Set up the 26 wall elements, which represent the thrust cylinders of the TBM, on the segment ring as shown in Fig. 8 (b).

(ix) Apply the acceleration due to gravity (9.81 m/sec^2).

(x) Apply isotropic pressure (500 kN/m^2) to the segment ring.

(xi) Remove the wall elements acting as thrust cylinders of the TBM.

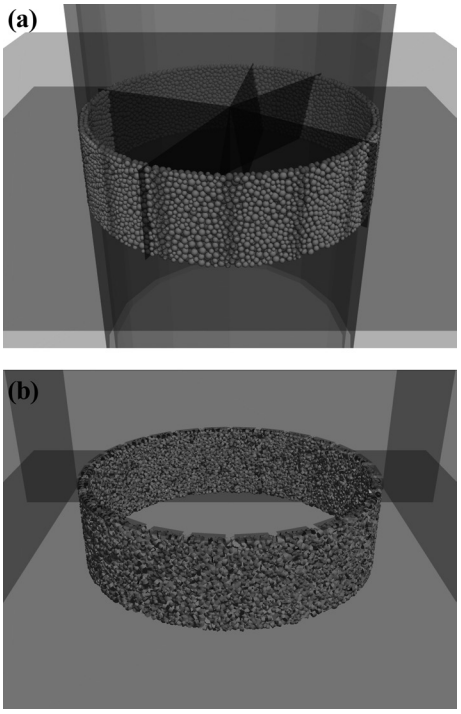

Fig. 8. Preparation of segments by DEM simulation. (a) Preparation of segments, (b) Representation of thrust cylinders.

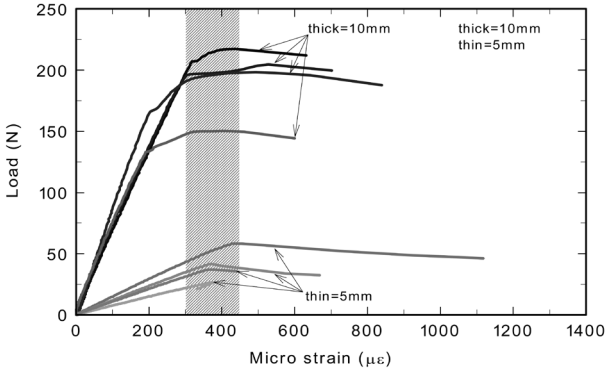

Fig. 9. Load against strain in simple bending tests (A-segment).

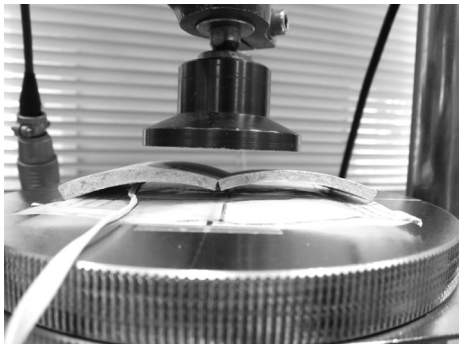

Fig. 10 Condition of A1-segment (thickness of segment: 5 mm) after loading in simple bending test.

All parameters used in the discrete element simulation are summarized in Table 3. These parameters were determined from the unconfined compression strength and elastic (ultrasonic) wave propagation velocities of the concrete specimens that were core-sampled from actual full-scale segments. The mean unconfined compression strength was 59.9 N/mm^2, while the mean elastic (ultrasonic) wave propagation velocities were V_{p_bm}= 4,760 m/sec and V_{s_bm}= 2,470 m/sec, indicating the P- and S-wave velocities, respectively. These values were slightly higher than the unconfined compression strength (46.2 N/mm^2) and the elastic (ultrasonic) wave propagation velocities (V_{p_bm}= 3,920 and V_{s_bm}= 2,340 m/sec) of the cement milk specimen used for the miniature segments. These values, however, had not much influence on the DEM parameters, such as the stiffness of the sphere elements, and the parallel-bonds that were determined using the determination manner, a procedure adopted and discussed in previous studies[7, 8].

Results and Discussions regarding Experimental Tests and Numerical Simulation

Results of simple bending tests

The variation of the load against the strain is shown in Fig. 9. The strain corresponding to the maximum load was observed at a strain level of around 300–450 με, which seemed to remain constant independent of the thickness of the segment. The value was related to the elastic modulus of the concrete that was prepared as described in this paper.

The conditions of the segments after the simple bending tests are shown in Fig. 10. Almost all segments failed into two parts along the central line in the direction of the width of the segment, given as 43.8 mm in Table 1.

Results of loading/unloading experimental tests

Figure 11 shows the development of stress and strain against elapsed time under isotropic pressure on the segment with 5 mm thickness. This was Case No.1 where the contact areas between K- and B-segments were not lubricated. In the figure, a compressive stress is shown as positive. In addition, the strain is expressed as positive when an arc length of the segment lengthens and that segment is pushed toward the outside; on the other hand, when an arc length of the segment shortens and that segment shrinks toward the inside, then the strain is expressed as negative.

As shown in the figure, with increasing isotropic pres-

Table 3. Parameters used in the simulation

Parameters		Notation	Value	Unit
Sphere element	Density	ρ_s	2,650	kg/m^3
	Mean radius	R	0.0408	m
	Normal stiffness	k^n	18.0	kN/mm
	Tangential stiffness	k^s	7.3	kN/mm
	Friction coefficient	μ	0.10–0.30	-
	Damping ratio	β^n, β^s	0.8	-
Ratio of radius of parallel-bond and sphere element		$\bar{\lambda}$	1.0	-
Parallel-bond	Normal stiffness	$\bar{k}^n$	480	N/mm^3
	Tangential stiffness	$\bar{k}^s$	130	N/mm^3
	Tensile strength	$\bar{\sigma}_c$	160	N/mm^2
	Shear strength	$\bar{\tau}_c$	160	N/mm^2

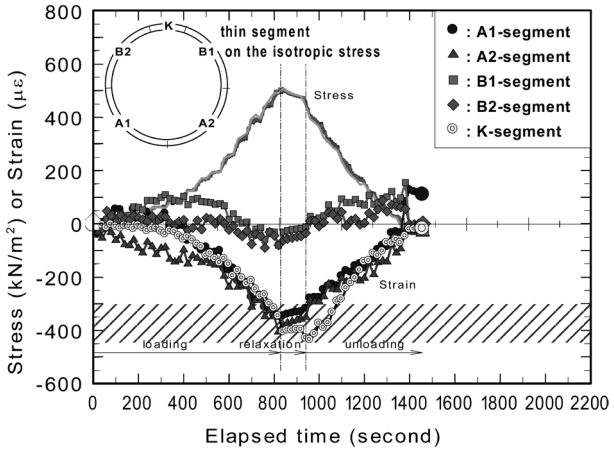

Fig. 11. Stress and strain against elapsed time (isotropic pressure, thickness of segment: 5 mm).

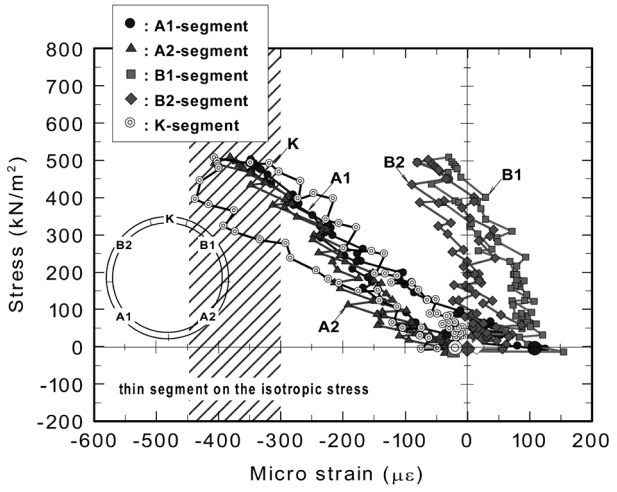

Fig. 12. Stress-strain behavior (isotropic pressure, thickness of segment: 5 mm).

sure, A1-, A2- and K-segments appeared to shrink toward the inside, while B1- and B2-segments seemed to behave in both manners (pushed out/shrink), and those strains increased/decreased around zero from the first to the last segment. With decreasing isotropic pressure, the strains in all segments approached zero value, showing elastic behavior.

The stress-strain behavior in Fig. 12 shows linear relationships that also expressed elastic behavior. The inclinations of the stress-strain relations for A1-, A2- and K-segments were generally the same and plotted lower than those for B1- and B-2 segments.

As seen in Fig. 13 which shows how the stress and strain vary with elapsed time on the 5 mm thick segment under anisotropic pressure, all segments showed negative strain until the stress of 500 kN/m^2 was reached. After that, we applied the anisotropic pressure to Bl8, Bl9 and $\bar{\text{B}}$l10; however, all the values being monitored by the load cells increased and therefore it was suggested that the increment in stress was supposed to be supported not only by A1- and B2-segments, but by all the segments. As seen in the plot of change in strain with increase in anisotropic pressure, the absolute values of the strains in A1- and A2-segments increased while those in B1- and B2-segments showed small values. The strain in K-segment rapidly increased with increase in anisotropic pressure; although unconfirmed, it was postulated that local stress concentrated in the segment through some gaps in the contact between the segments because the corners and the shapes of the segments did not exactly correspond to the design of the miniature segmental ring which had few minor lack of corners and shapes.

Figure 14 shows the stress-strain behavior under anisotropic pressure on the segment with 5 mm thickness. The

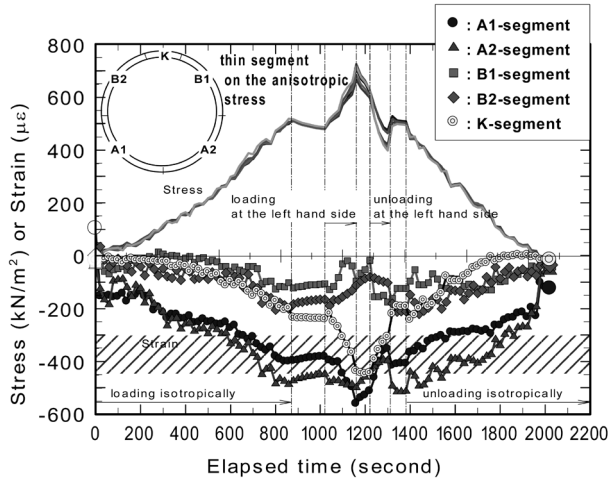

Fig. 13. Stress and strain against elapsed time (anisotropic pressure, thickness of segment: 5 mm).

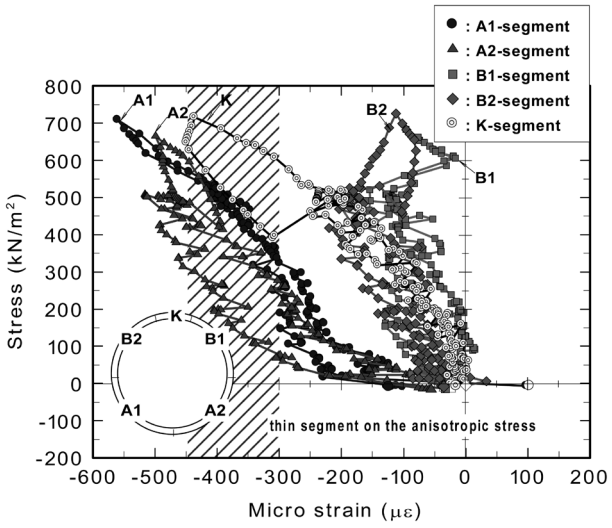

Fig. 14. Stress-strain behavior (anisotropic pressure, thickness of segment: 5 mm).

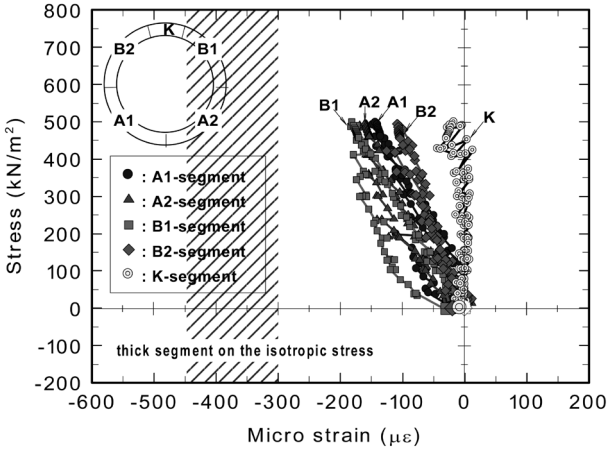

Fig. 15. Stress-strain behavior (isotropic pressure, thickness of segment: 10 mm).

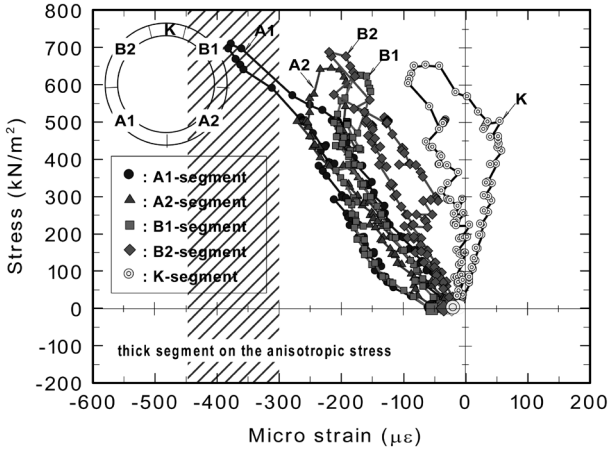

Fig. 16. Stress-strain behavior (anisotropic pressure, thickness of segment: 10 mm).

slopes of the stress-strain relation for A1-, A2- and K-segments were gentler than those of the other segments, similar to the tendency described above. In addition, a negative strain of around −125 με remained in A1-segment after unloading.

Next, the stress-strain responses under isotropic and anisotropic pressures of the 10 mm thick segments are shown in Figs. 15 and 16, respectively, representing Case 2 where the contact areas between B- and K-segments were not lubricated. The inclinations of the stress-strain relation under isotropic pressure for A1-, A2-, B1- and B2-segments corresponded well. The absolute value of the strain showed maximum value of around 200 με, which was lower than that observed in the 5 mm thick segment (around 400 με). Regarding K-segment, the strain generated was very small and very close to zero. The K-segment had originally shorter arc length than the other segments and it was also thicker, and therefore its strength for the same amount of pressure was supposed to be higher than that of the thinner one.

During anisotropic loading/unloading on the 10 mm thick segment, the strain became larger in A1-segment and the inclinations of stress-strain relation were very similar in all segments, except K-segment. In addition, after unloading, the strains remained close to zero and hence the segments appeared to behave elastically. Therefore, it was suggested that thick segments would have greater stability against anisotropic pressures.

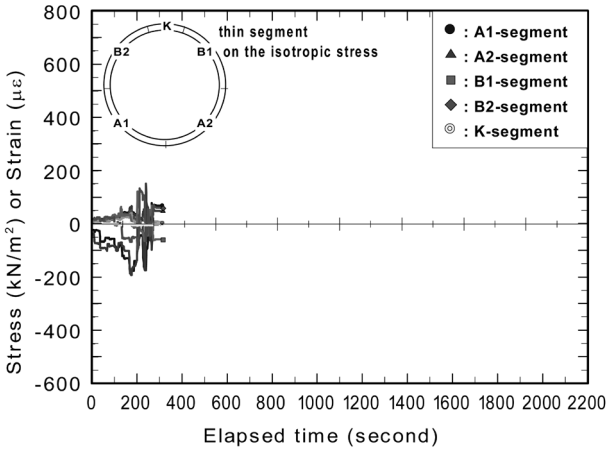

Fig. 17. Stress and strain against elapsed time (thickness of segment: 5 mm, lubricated).

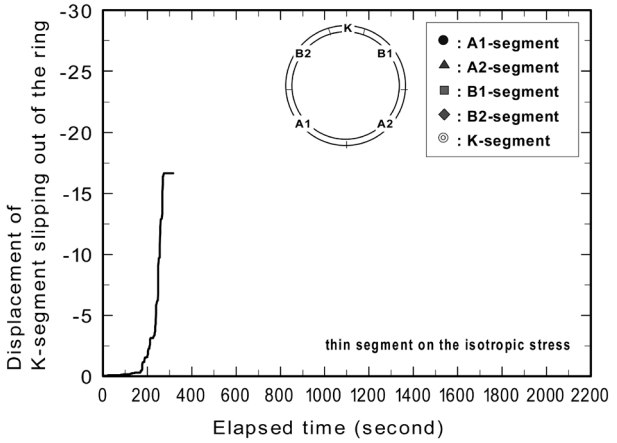

Fig. 18. Displacement of K-segment slipping out of the ring against elapsed time (thickness of segment: 5 mm, lubricated).

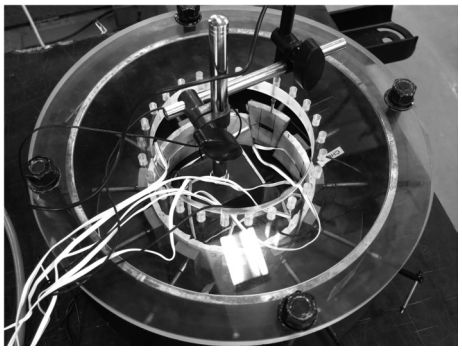

Fig. 19. K-segment slipping out of the ring (thickness of segment: 5 mm, lubricated).

In Figs. 14, 16, 17 and 18, we showed the range of failure strain level, i.e. between −450 to −300 με, with dashed zones. Referring to Fig. 11 which showed the failure strain level as a result of the simple bending tests to be positive, we assumed that the segments would fail at the same strain level but on the negative side. In this paper, we defined that the failure strain level to be ±300 to ±450 με. When the strain level under isotropic and anisotropic pressures for thin and thick segments in loading/unloading tests were compared with the failure strain level observed in the simple bending tests, the thick segments under isotropic and anisotropic pressures seemed to have lower values, i.e. with failure strain level of −450 to −300 με. On the other hand, the thin segments under anisotropic pressure exceeded the failure strain level of −450 to −300 με, i.e., anisotropic pressure would be severe for thin segmental rings. It was, however, noted that the axial force acting on the segmental ring was around 2,220 N, which was calculated using the theoretical conventional method under an anisotropic pressure of 700 kN/m^2, although the axial force was very close to 0 N in the simple bending tests.

In Case Nos. 3 and 4, the segments were lubricated for both 5 mm thick and 10 mm thick cases, respectively; both K-segments slipped out of the segment rings under very low isotropic pressure (less than around 100 kN/m^2), and then the pressure could not be increased further after that as any increment in pressure would increase the displacement of the K-segment as it slipped out of the rings (Figs. 17–19).

Results of numerical simulation

For single bending tests, previous comparison made between the numerical simulations and the experimental test results on the load versus strain relationship showed good agreement in the behavior, except at failure strain level[9]. In this paper, we presented only the results of the simulation for Case No. 3 of the experimental tests. Figure 20 shows the results of simulation where the friction coefficients between the sphere elements (segments) were varied as 0.1, 0.2 and 0.3. As seen in the images, the K-segment slipped-out of the ring when the friction coefficients were 0.1 and 0.2, although the displacement decreased with the increase in friction coefficient.

Conclusions

From the simple bending tests, the segment was observed to have better resistance against the bending load with increase in thickness. The failure strain, which showed the maximum resistance against bending, seemed

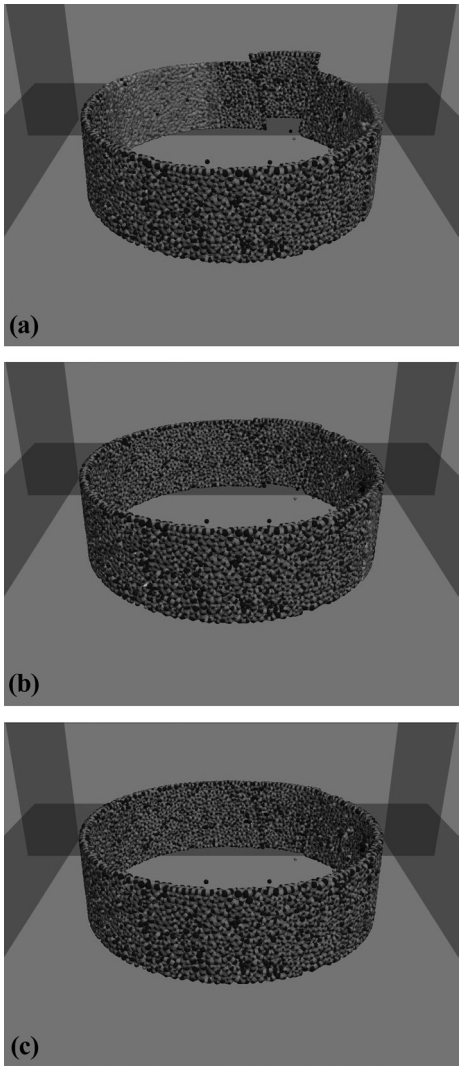

Fig. 20. K-segment slipping out of the ring. (a) friction coefficient of 0.1, (b) friction coefficient of 0.2, (c) friction coefficient of 0.3.

to be constant such that the failure strain was independent of the thickness because the failure strain should be a function of the strength capacity of the concrete.

From both experimental tests and numerical simulations of the behavior of a segmental ring, it was suggested that there was a higher possibility that the segments would suffer some deformation/damage under anisotropic pressure when the thickness of the segments was decreased.

In addition, the friction between the segments should not be counted on. Instead, each segment should be physically connected to each other, say with bolts, etc. The segmental ring should be stable with the application of earth and water pressures, even if only acting as a single segmental ring.

Acknowledgement

The experimental tests presented in this paper had been conducted with the assistance of Risako Nakagawara and Takeshi Yamamoto, both undergraduate students of the College of Industrial Technology, Nihon University at that time. We are very grateful to them for their contributions.

References

1) Kimata H, Nakayama T, Tsuno K, Kayukawa K and Konishi S (2013) Investigation of contact between shield and segment under excavation on segment crack based on numerical analysis. J Jpn Soc Civ Eng Div F1 (Tunnel Engineering), **69**, 73–88 (In Japanese).
2) Saito J, Kurosaki S, Takahashi A, Takeuchi T, Koizumi A (2007) Damage factors of the segment during tunneling in a large depth shield tunnel, J Jpn Soc Civ Eng Div F **63**, 200–11 (In Japanese).
3) National Institute of Occupational Safety and Health Japan. Industrial accident due to the collapse and submergence during TBM-tunnel construction under seabed, Industrial Accident Analysis Report, https://www.jniosh.go.jp/publication/pdf/saigai_houkoku_2016_02.pdf#zoom=100. Accessed February 27, 2018 (In Japanese).
4) Japan Society of Civil Engineers, Japan Sewage Works Association (2001) Standard segments for shield tunneling construction—segments for sewer shield tunneling construction—JSWAS A-3, 4–2001, p428, Japan Sewage Works Association, Tokyo.
5) Yuasa Y, Masuno M, Koizumi A (2010) Study on watertightness of RC segment for underground river shield tunnel. J Jpn Soc Civ Eng Div F **66**, 578–92 (In Japanese).
6) Kimura M, Adachi T, Kobayashi H (1995) Centrifuge model tests on ultimate behavior of laterally loaded reinforced concrete piles, Annuals, Disaster Prevention Research Institute. Kyoto Univ **B-2**, 67–82 (In Japanese).
7) Kikkawa N, Hori T, Itoh K, Mitachi T (2013) Study on a determination manner of Discrete Element Method parameters in a bonded granular material. Jpn Geotech J Elsevier **8**, 221–37 (In Japanese). [CrossRef]
8) Kikkawa N, Itoh K, Mizutani T, Hori T, Toyosawa Y, Pender MJ, Orense RP (2014) Blasting of cemented granular material and discrete element simulation of the process, IS-Cambridge 2014, Geomechanics from Micro to Macro, 411–16.
9) Kikkawa N, Imai S, Hiraoka N, Itoh K (2017) Bending tests of segmental model and its discrete element simulation, Proceedings of Tunnel Engineering, Japan Society of Civil Engineers, CD-ROM, II-9, pp1–9 (In Japanese).